RSC Advances

ROYAL SOCIETY OF CHEMISTRY

www.rsc.org/advances

Journal Name

ARTICLE

A high-performance ambipolar organic field-effect transistors based on a bidirectional π-extended diketopyrrolopyrrole under ambient conditions

Received 00th January 20xx,
Accepted 00th January 20xx

DOI: 10.1039/x0xx00000x

www.rsc.org/

Jinfeng Bai, [a]† Yucun Liu,[a]† Sangyoon Oh,[b] Wenwei Lei,[a] Bingzhu Yin*[a], Sooyoung Park*[b] and Yuhe Kan*[c]

A novel bidirectional π–extended 2,5-dihydro-1,4-dioxo-3,6-di-2-thienyl-1,4-diketopyrrolo[3,4-c]pyrrole derivative (**DPP-2T**) with the 4-(2,2-dicyanovinyl)phenyl group, (**DPP-2T2P- 2DCV**), has been synthesized and characterized in order to achieve a high-performance organic semiconductor. The HOMO/LUMO energies of **DPP-2T2P- 2DCV** were estimated to be -5.36 and -3.81 eV, respectively, based on their redox potentials, which were very similar to the other bidirectional π-extended **DPP-2T** analogue **DPP-4T-2DCV**. The calculated HOMO/LUMO values (HOMO: –5.43 eV, LUMO: -3.56 eV) based on the optimized geometry agreed well with the experimental values. **DPP-2T2P-2DCV** exhibits ambipolar TFT response with reasonably balanced electron and hole mobilities of 0.168 $cm^2 V^{-1} s^{-1}$ and 0.015 $cm^2 V^{-1} s^{-1}$ by solution process, respectively, which is the best result for solution processable DPP-based ambipolar small molecule semiconductors measured under ambient atmosphere.

Introduction

Organic field-effect transistors (OFETs) have been the focus of attention for many researchers in the past two decades due to their great potential as fundamental elements in electronic devices, such as, radio frequency identification (RFID) tags, smart cards,[1] electronic papers,[2] displays,[3] sensors and so on.[4-6] Extensive studies of OFETs have resulted in the development of organic semiconductors rivalling or surpassing the electrical performance of amorphous silicon,[7-15] and combining low-cost processability/printability with excellent mechanical flexibility.[7,16-19]. As a result, a number of p-type organic semiconductors with hole mobilities (μ_h) up to 30 $cm^2 V^{-1} s^{-1}$ have been investigated.[20-22] Also, n-type organic semiconductors have been reported with electron mobilities (μ_e) reaching 6.0 $cm^2 V^{-1} s^{-1}$.[23-27] In comparison, organic ambipolar semiconductors with high and balanced hole/electron mobilities are still limited. However, ambipolar semiconductors capable of efficiently transporting both holes and electrons by simply changing the bias voltage are extremely desirable for complementary-like electronic circuit fabrication, [19, 28] and for light-emitting tran-sistors.[29-32] For this reason, intense efforts have been made in recent years to the development of high-performance ambipolar small molecules and polymers. Among the most often used building blocks for ambipolar organic semiconductor design is the diketopyrroloyrrole (DPP) core. The electron-deficient nature of DPP provides low energy LUMO levels, hence allowing the synthesis of low band-gap donor–acceptor systems when combined with thiophenic moieties having high-energy HOMOs, which have been shown to be excellent candidates for organic electronics[27, 33-38] and photonics.[39-43] So far, a family of soluble small organic molecules containing a diketopyrrolopyrrole (DPP) core have been synthesized. Some DPP-based polymers have recently yielded ambipolar transport with mobilities surpassing 1 $cm^2 V^{-1} s^{-1}$.[35, 44-49] In comparison to DPP polymers, DPP-based small molecules have been studied to a far less extent; some also display ambipolarity, but with more modest performance, on the order of 10^{-2} $cm^2 V^{-1} s^{-1}$.[50-52] It is only recently that the introduction of dicyanovinyl units on DPP–oligothiophene cores (**DPP-4T-2DCV** and **2DPP-6T-2DCV**) (see Fig. 1) has resulted in high-performance ambipolar semiconductors with hole and electron mobilities of ~0.16 $cm^2 V^{-1} s^{-1}$ and ~0.02 $cm^2 V^{-1} s^{-1}$, respectively.[53] This should be due to the strong electron-withdrawing dicyanovinyl units on DPP–oligothiophene, which effectively lower the LUMO and, hence, improve electron injection from the contact electrodes. In this regard, a breakthrough progress has been made in improvement of ambipolar mobilities by inserting 1,2-difluorovinyl between dithienyl-DPP core and benzo[b]-thiophene. Remarkably, OFET devices based on thin films of

[a] *Key Laboratory of Natural Resources of Changbai Mountain & Functional Molecules, Yanbian University, Ministry of Education, Yanji, Jilin 133002, PR China. E-mail: zqcong@ybu.edu.cn*
[b] *Director of Center for Supramolecular Optoelectronic Materials (CSOM) Professor of Materials Science & Engineering, Seoul National University email : parksy@snu.ac.k*
[c] *Jiangsu Province Key Laboratory for Chemistry of Low-Dimensional Materials, School of Chemistry and Chemical Engineering, Huaiyin Normal University, Huaian, China. E-mail: yhkan@yahoo.cn*
† These authors contributed equally.
Electronic Supplementary Information (ESI) available: [details of any supplementary information available should be included here]. See DOI: 10.1039/x0xx00000x

the bidirectional π-extended dithienyl-DPP derivative (**DPP-2F**) exhibit ambipolar semiconducting properties with μ_h and μ_e values reaching 0.42 and 0.80 $cm^2\ V^{-1}s^{-1}$, respectively.[54] However, their OFET devices also have to be measured under inert conditions or vacuum in order to observe ambipolar behaviour, even when the electron-deficient dicyanovinyl or difluorovinyl unit was introduced to further reduce the LUMO energy level of the DPP derivatives. So far, to our knowledge, only one DPP-based conjugated oligomer exhibits field-effect hole and electron mobilities of 0.066 and 0.033 c $cm^2\ V^{-1}\ s^{-1}$, respectively, when the devices are fabricated and measured in the air.[55]

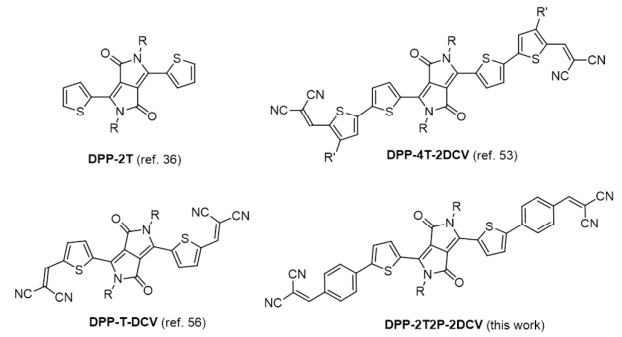

Fig. 1 Some representative DPP-based small molecules for organic thin-film transistors and the chemical structures of **DPP-2T2P-2DCV**.

With these advances in mind, we displace the terminal attached thiophene units of **DPP-4T-2DCV** (Fig. 1) with phenylene units to synthesize target compound **DPP-2T2P-2DCV** (Scheme 1). The molecular design is based on the following considerations: 1) the introduction of dicyanovinyl is expected to lower the LUMO energy by taking advantage of the electron-withdrawing feature of cyano group and, accordingly, **DPP-2T** may behave as an ambipolar semiconductor;

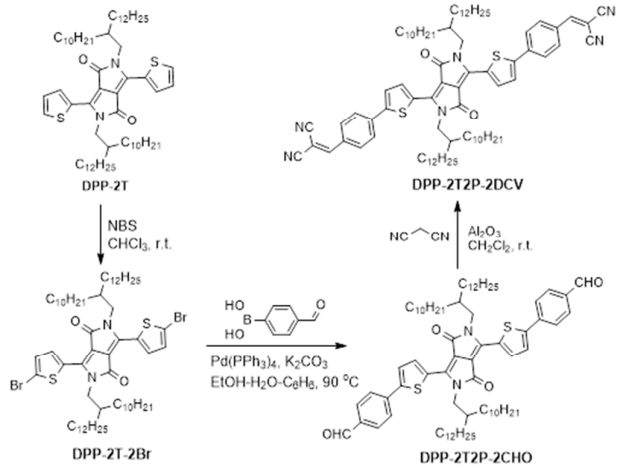

Scheme 1 Synthetic approach for the preparation of **DPP-2T2P-2DCV.**

2) insertion of phenylene unit between **DPP-2T** and dicyanovinyl moieties may extend the conjugation length, and thus, lower the band gap and promote intermolecular π–π stacking. The electrical performances of **DPP-2T2P-2DCV** have been tested in OFET devices, as expected, showing ambipolar reasonable balanced field effect mobilities of up to ~0.1680 and ~0.0154 $cm^2\ V^{-1}\ s^{-1}$ for electron and hole transport under ambient conditions, respectively. In here, we present the synthesis and characterization of the novel DPP derivative, **DPP-2T2P-2DCV**, fabrication of OFETs based on their spin-coated thin films, and FET characteristics of the devices.

Results and discussion

3.1 Synthesis, characterization and thermal properties

Firstly, long branched 2-decyltetradecyl chains were introduced into the nitrogen centers of the DPP-2T monomer to increase solubility and processability from solution. The dibrominated **DPP-2T-2Br** was conveniently prepared by bromination using N-bromosuccinimide (NBS) in anhydrous $CHCl_3$ at room temperature and the crude product was purified by column chromatography. Subsequent Suzuki coupling of the dibromide with 4-formylphenylboronic acid afforded intermediate **DPP-2T2P-CHO** in the presence of $Pd(PPh_3)_4$ and K_2CO_3 in a mixture of solvent ethanol-water-benzene. Target compound **DPP-2T2P-2DCV** was synthesized by conventional Knoevenagel reaction between intermediate **DPP-2T2P-CHO** and malononitrile in the presence of Al_2O_3 in 90% yield (Scheme 1).

Target compound possesses excellent solubility in common organic solvents and the new compounds were characterized by NMR and optical spectroscopy, mass spectrometry techniques as well as elemental analysis. And, the IR spectra of both of these compounds clearly evidence the presence of the carbonyl groups and cyano groups at 1709 and 2221 cm^{-1}, respectively, in conjugation with the inner core (Fig. S1).

Thermal properties of the **DPP-2T2P-2DCV** were evaluated by differential scanning calorimetry (DSC) and thermos-gravimetric analysis (TGA) under nitrogen (Fig. S2). The results reveal that **DPP-2T2P-2DCV** is thermally stable below 300 °C and the decomposition temperature (T_d) at 5% weight loss is above 336 °C, which is high enough for device fabrication.

3.2 Photophysical properties and HOMO/LUMO Energies

The characteristic feature of the primary chemical structure and the molecular stacking effect of **DPP-2T2P-2DCV** in the solid-state was analyzed by UV-vis absorption spectroscopy in both the solution and the thin solid film state, showing the typical features of DPP derivatives.[53, 56] As shown in Fig. 2a, the absorption spectrum is characterized by two principal absorptions, around 413 nm due to the thiophene-benzene portion of the molecule and another, more intense band at 613 nm with a vibronic absorption shoulder at 651 nm, likely involving the DPP unit together with the surrounding thiophenes. The calculated absorption wavelengths of **DPP-2T2P-2DCV** is 595 nm and 368 nm, respectively, which are slightly lower but in good agreement with the experimental

results (Fig. S3, Table S1). The sequentially alternating intramolecular electron donor (thiophene-benzene) and acceptor (DPP and DCV) moieties in molecules probably produced an intramolecular charge transfer (ICT), which substantially decreased the energy band gap and induced the well resolved vibronic peak at lower energy region (651 nm). In the solid-state film, the absorption spectrum of **DPP-2T2P-2DCV** broadly spanned the long wavelength region (550–900 nm). From solution to film, the absorption maxima had a bathochromic shift by 146 nm, indication of the planarization of the π-backbone. On the basis of onset absorption wavelength of thin film, the band gap (E_g^{opt}) was estimated to be 1.51 eV.

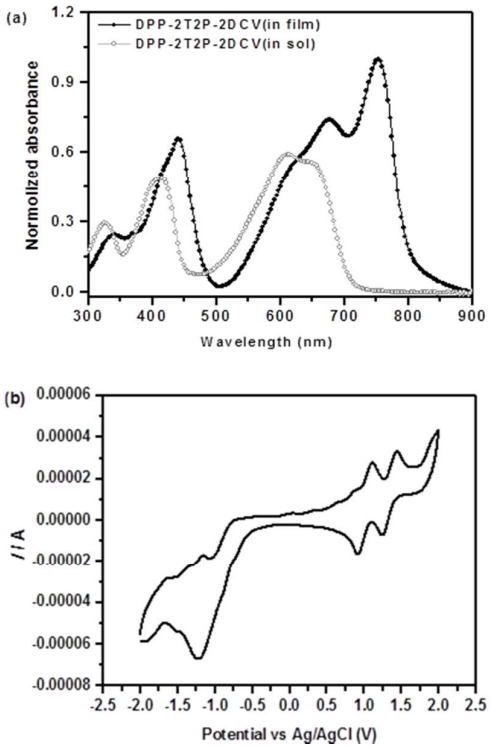

Fig. 2 (a) UV-Vis absorption spectra of **DPP-2T2P-2DCV** in the solution and thin film states and (b) cyclic voltammogram in CH_2Cl_2 solution. Potentials are reference versus Ag/AgCl.

Cyclic voltammetry (CV) measurements were conducted in order to calculate the HOMO and LUMO energy levels. The cyclic voltammogram for **DPP-2T2P-2DCV** is shown in Fig. 2b. The anodic and cathodic scans showed that the onsets of oxidation and reduction for **DPP-2T2P-2DCV** occurred at 0.95 and -0.6 eV, respectively, and thus the HOMO and LUMO levels were calculated to be -5.36 eV and -3.81, respectively, using the empirical equation: HOMO = - (E_{onset}^{ox} + 4.41) eV. On the basis of their onset oxidation and onset reduction, the band gap of **DPP-2T2P-2DCV** was estimated to be 1.55 eV, As can be seen, the electrochemical band gap calculated from the oxidation and reduction potential onsets in solution is slightly higher than the optical band gap calculated from the onset of the optical absorption in thin films. Explanations for this can be found in the fact that the electrochemical experiment takes place in solution, where stacking of the molecules is absent, resulting in a higher bandgap.[57] However, E_g^{CV} is relatively lower compared with E_g^{opt} (1.69 eV) in solution, We think that the result have relation to the test concentration in the different environment. Interestingly, the insertion of the phenylene group between DPP-2T and dicyanovinyl moiety, instead of thiophene, resulted in an ~0.14 eV drop for LUMO and E_g compared with those of the previously reported thiophene analogue (LUMO = -3.68 eV, E_g^{CV} = 1.69 eV).[53]

DFT calculations were performed to rationalize the structure and HOMO/LUMO energies of **DPP-2T2P-2DCV**. To simplify the calculations, alkyl chains were replaced with ethyl groups. The HOMO orbital of **DPP-2T2P-2DCV** is mainly localized in the entire dithienyl-DPP moiety, whereas its LUMO orbital is uniformly distributed throughout the whole molecular backbones, as depicted in Fig. 3. The calculated HOMO, LUMO and E_g values for **DPP-2T2P-2DCV** (HOMO: –5.43 eV, LUMO: 3.56 eV, E_g: 1.87 eV) based on the optimized geometry agreed well with the experimental values. The closing of the gap between the reduction and oxidation potentials could lead to an ambipolar character. These results suggest that **DPP-2T2P-2DCV** is highly suitable for realizing high-mobility ambipolar OFETs.

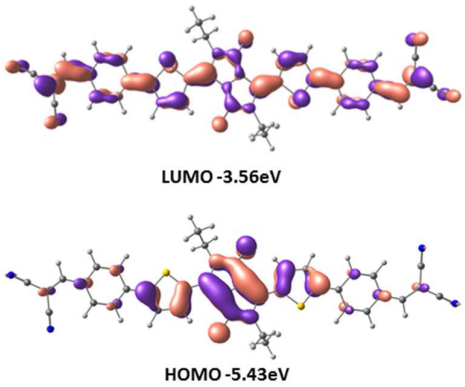

Fig. 3 Kohn-Sham orbitals of **DPP-2T2P-2DCV** at the B3LYP/6-31G* level of theory.

3.3 Thin film properties and charge transport

The thin films of **DPP-2T2P-2DCV** were deposited on octadecyltrichlorosilane (ODTS) treated SiO_2/Si substrates by spin-coating their $CHCl_3$ solutions (20 mg/mL), and characterized by XRD and AFM techniques. The crystallinity and long range packing order of **DPP-2T2P-2DCV** thin films were studied by out-of-plane grazing incidence X-ray diffraction and data are shown in Fig. 4A. As seen in Fig. 4A, the semiconductor shows modest crystalline feature. The XRD of **DPP-2T2P-2DCV** films after thermal annealing at 90 °C displayed a relatively strong first-order reflection and a weak second-order reflection with *d* spacings of 2.21 and 1.12 nm, respectively, which were roughly in the ratio of 2:1 and agreed with (100) and (200)

reflections of a lamellar packing structure. Length of the molecule along the branched alkyl chains is approximately 22.4 Å, according to analysis of CPK model, which is close to first-order *d* spacing (22.1 Å). Taking this into consideration, the molecular orientation in the solid films could be edge-on packing conformation with the alkyl groups standing on the substrate. Furthermore, the occurrence of the weak second-order lamellar diffraction features in the semiconductor film suggests minimal long-range crystallinity. However, the two diffraction peaks remain almost unaltered and no new signals emerge upon further increasing the annealing temperatures to 120 °C, although the second-order signal at 8.06 ° is slightly enhanced (Fig. 4A).

The topologies of the **DPP-2T2P-2DCV** thin films were also analyzed by tapping mode AFM. Fig. 4B shows the AFM images for as-cast and annealed films at different temperatures. Remarkably, the as-cast **DPP-2T2P-2DCV** films show relatively larger void areas and more distinct grain boundaries between crystalline domains, whereas the films that were annealed at 90 °C for 15min exhibits interconnected granular domains with more smooth surfaces. Further increasing the annealing temperature to 120 °C, however, the film morphology does not have obvious variation. Although the debate is still open, interconnected granular domains with more smooth surfaces are usually related to enhanced device performance.

The device performances were measured under ambient conditions. All the performance data were obtained based on more than 10 different OFETs. Based on the transfer and output characteristics shown in Fig. 5, a thin film of **DPP-2T2P-2DCV** shows ambipolar semiconducting behavior in air. The average and maximum field effect mobilities, along with the average threshold voltages are listed in Table 1. The electron

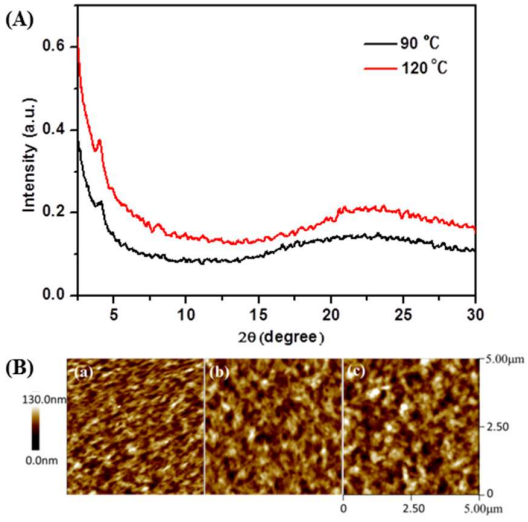

Fig. 4 (A) Out-of-plane X-ray diffraction patterns and (B) tapping-mode AFM images recorded for **DPP-2T2P-2DCV** under different annealing temperature. (a) 25 °C, (b) 90 °C and (c) 120 °C.

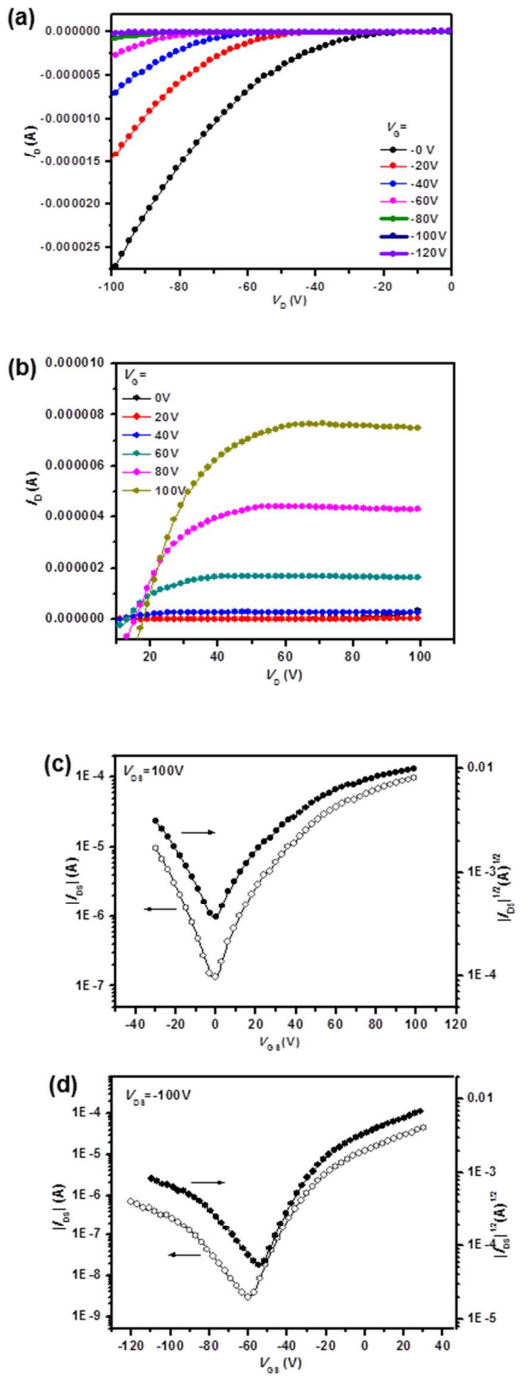

Fig. 5 Typical output (a, b) and transfer (c, d) curves of the OFET devices based on **DPP-2T2P-2DCV** films with thermal annealing at 120 °C for 1 h.

and hole mobilities of the as-prepared OFET with a thin film of **DPP-2T2P-2DCV** were deduced to be 8.43×10^{-2} and 8.49×10^{-3} $cm^2\ V^{-1}\ s^{-1}$. Both μ_e and μ_h increased and reached 0.157 and 0.014 $cm^2\ V^{-1}\ s^{-1}$ upon removal of the solvents at 90 °C for 1.0 h

in air (see Table 1). Moreover, both μ_e and μ_h were further enhanced by increasing the annealing temperature and reached 0.168 and 0.015 $cm^2 V^{-1} s^{-1}$, respectively, after annealing at 120 °C for 1.0 h. However, the enhancement of μ_h and μ_e was not remarkable. These OFET data are well parallel to the fact that both the XRD patterns and AFM images of thin films of **DPP-2T2P-2DCV** are almost unaltered when annealing at different temperatures (90 °C and 120 °C). To our knowledge, the ambipolar μ_e and μ_h values of **DPP-2T2P-2DCV** are among the highest in DPP-based small molecules under ambient condition. It is worth noting that there is no improvement on charge mobilities of the OFETs observed under inert conditions (Fig. S4). Actually, inserting of phenylene groups between DPP-2T and DCV units of **DPP-T-DCV**, which is a recently published n-type semiconductor with a truncated π-core,[56] results in the increase of HOMO energy. Importantly, this extension of π-conjugation switches the transport characteristics from unipolar n-type conduction to ambipolarity.

Table 1 FET properties of compound **DPP-2T2P-2DCV**.

Temp./°C	μ_e[a] $cm^2/V^{-1}s^{-1}$	V_T/V	μ_h[a] $cm^2/V^{-1}s^{-1}$	V_T/V	I_{on}/I_{off}
RT	0.084 (0.058)	6	0.008 (0.005)	-30	10^2-10^3
90	0.157 (0.061)	16	0.014 (0.005)	-34	10^1-10^2
120	0.168 (0.062)	13	0.015 (0.005)	-43	10^2-10^3

[a] The mobilities were provided in "highest (average)"form, and the performance data were obtained based on more than 10 different OFETs.

To further understand the charge transport process we also calculated the internal reorganization energies of the neutral molecule under positive and negative charging. This theoretical parameter is related to geometrical relaxation accompanying charge transfer, and small values are desirable for efficient charge transport.[58] Intramolecular reorganization energies for electron/ hole transport were estimated to be 0.228/0.237 eV for **DPP-2T2P-2DCV**. The lower values found for both electron and hole transport is in good agreement with the higher electrical performance. To estimate the intermolecular transfer integral of semiconductor, which is a main factor for influence the mobility, many attempts were made to grow single crystals but without success, which is probably due to the presence of the bulky alkyl chains in the conjugated skeletons.

Experimental

Materials and general methods

Commercially available compounds were used without further purification. Solvents were dried according to standard procedures. All reactions were magnetically stirred and monitored by thin-layer chromatography (TLC) using QingDao GF254 silica gel coated plates. NMR spectra were recorded on a Bruker AV-300 Spectrometer (300 MHz for ^{1}H and 75 MHz for ^{13}C), and chemical shifts were referenced relative to tetramethylsilane (H/C = 0). UV-vis spectra were recorded with a Shimadzu UV-2550 spectrophoto-meter.Cyclic voltammetric studies were carried out on a Potentiostat/Galvanostat 273A instrument in CH_2Cl_2 (1:1, c = 1×10^{-3} M) and 0.1 M Bu_4PF_6 as the supporting electrolyte and scan rate is 100 mV S^{-1}. Counter and Working electrodes were made of Pt and Glass-Carbon, respectively, and the reference electrode was calomel electrode (Ag/AgCl). MALDI-TOF mass data were obtained by a Shimadzu AXIMA-CFR^{TM} *plus* mass spectrometry, using a 1, 8, 9-anthracenetriol (DITH) matrix. The thermal stability of target compounds were characterized by Shimadzu DTG-60H thermogravimetric analyzer. A Perkin-Elmer Pyris Diamond differential scanning calorimeter was used to determine the thermal transitions, which were reported as the maxima and minima of their endothermic or exothermic peaks; the heating and cooling rates were controlled at 10 °C min^{-1}.

Synthesis and characterization

All solvents were purified and dried according to literature methods. Compounds **DPP-2T** and **DPP-2T-2Br** were synthesized according to the literature procedure.[36]

Synthesis of DPP-2T2P-2CHO: A mixture of **DPP-2T-2Br** (0.0980 g, 0.09 mmol), 4-formylphenylboronic acid (0.0519 g, 0.36 mmol), $Pd(PPh_3)_4$ (0.0120 g, 0.108 mmol) and K_2CO_3 (0.0862 g, 0.648 mmol) in a mixture of EtOH/H_2O/C_6H_6 (1 : 1 : 2, 10 mL) was stirred under argon atmosphere at 90 °C for 24h. After cooling, the resulting mixture was dissolved in CH_2Cl_2, washed with water and dried over $MgSO_4$. After evaporation of the solvent, the crude product was purified by recrystallization (C_6H_6/CH_3OH) to give **DPP-2T2P-2CHO** as a dark-blue solid (0.0870 g, 85%). M.p.130-131. ^{1}H-NMR ($CDCl_3$, 300MHz): δ 10.04 (s, 2H), 9.00 (d, *J* = 4.1, 2H), 7.98 (d, *J* = 7.9 Hz, 4H), 7.88 (d, *J* = 7.9 Hz, 4H), 7.65 (d, *J* = 4.1 Hz, 2H), 4.12 (d, *J* = 7.6 Hz, 4H), 2.01 (brs, 2H), 1.34-1.26 (m, 80H), 0.88-0.83 (m, 12H) ppm. ^{13}C-NMR (75 MHz, $CDCl_3$): δ 191.2, 161.6, 147.5, 139.6, 138.7, 13,6.7, 136.0, 130.6, 126.4, 126.2, 113.7, 112.7, 109.3, 82.5, 77.4, 77.2, 77.0, 76.6, 53.4, 46.4, 38.0, 31.9, 30.0, 29.7, 29.4, 26.4, 22.7, 14.1 ppm. FTIR (KBr) ν (cm^{-1}): 1709 cm^{-1}. MALDI-TOF MS m/z 1180.50 (M^+, 100). Elemental analysis: calcd for $C_{76}H_{112}N_2O_4S_2$: C, 77.24; H, 9.55; N, 2.37. Found: C, 77.45, H, 9.57; N, 2.25%.

Synthesis of DPP-2T2P-2DCV: A mixture of **DPP-2T2P-2CHO** (0.0435 g, 0.04 mmol), malononitrile (0.0146 g, 13.9 μL) and Al_2O_3 (0.0394 g, 42 mmol) in dichloromethane (12 mL) was stirred for 3h at room temperature. The catalyst Al_2O_3 was filtered off and the solvent was removed under reduced pressure. The crude product was purified by recrystallization (C_6H_6/CH_3OH) to give **DPP-2T2P-2DCV** as a dark- green solid (0.0423 g, 90%). M.p. 196 °C (by DSC). ^{1}H NMR($CDCl_3$, 300 MHz): *δ* 8.98 (d, *J* = 4.2 Hz , 2H), 7.98 (d, *J* = 8.4 Hz, 4H), 7.83 (d, *J* = 8.4 Hz, 4H), 7.74 (s, 2H), 7.64 (d, *J* = 4.2 Hz, 2H), 4.07 (d, *J* = 7.6 Hz, 4H), 1.96 (brs, 2H), 1.23 (m, 80H), 0.92-0.87 (m, 12H) ppm. ^{13}C NMR ($CDCl_3$, 75 MHz): δ 161.5, 158.1, 146.9, 139.7, 138.7, 136.9, 131.7, 131.2, 130.8, 126.7, 126.5, 113.7, 112.7, 109.3, 82.5, 77.4, 77.2, 77.0, 76.6, 53.4, 46.4, 38.0, 31.9, 30.0, 29.7, 29.4, 26.4, 22.7, 14.1 ppm. FTIR (KBr) ν (cm^{-1}): 2222 cm^{-1}.

MALDI-TOF MS m/z 1277.80 ([M+1]$^+$, 100). Elemental analysis: calcd for $C_{82}H_{112}N_6O_2S_2$: C, 77.07; H, 8.83; N, 6.58. Found: C, 77.30; H, 5.69; N, 6.46%.

OFET device fabrication and characterization

Top contact OFETs were fabricated. A heavily doped n-type Si wafer and a layer of dry oxidized SiO_2 (300 nm, with roughness lower than 0.1 nm and capacitance of 11 nF cm^{-2}) were used as gate electrode and gate dielectric layer, respectively. Octadecyltrichlorosilane (ODTS) was introduced onto the substrates as a self-assembled monolayer (SAM) in vapor phase in vacuum oven. The substrates were rinsed with acetone and isopropyl alcohol respectively for 10 min under ultrasonicator, and then 20min UV (360 nm) O_3 treatment was applied. Organic semiconducting materials were dissolved in chloroform (20 mg/mL) and the solution of samples were spin coated at 2500rpm onto ODTS treated substrate in nitrogen filled glove box under ambient condition. 50nm thick source-drain gold electrodes were thermally deposited onto semiconducting layer in a vacuum chamber. (Deposition rate was 0.1~0.2k Å/s). The annealing process was carried out in vacuums for 1.0 hr at each temperature. The *I-V* characteristics of all OFETs were measured under ambient condition by Keighley 4200 SCS instrument which is connected with probe stations. The mobility and threshold voltage were derived from saturation region of transfer curve, and source-drain channel widths of devices were checked by optical microscope for calculation of charge carrier mobility.

The mobility of the OFETs in the saturation region was extracted from the following equation:

$$I_{DS}=\mu Ci(V_{GS}-V_{Th})^2W/2L$$

where I_{DS} is the drain electrode collected current; L and W are the channel length and width, respectively; μ is the mobility of the device; Ci is the capacitance per unit area of the gate dielectric layer; V_{GS} is the gate voltage, and Vth is the threshold voltage. The Vth of the device was determined by extrapolating the $(I_{DS}, sat)^{1/2}$ vs. V_{GS} plot to I_{DS} = 0.

Conclusions

In summary, **DPP-2T2P-2DCV**, a highly electron-deficient semiconductor, was prepared in a simple way and used for high performance OFETs. Based on the performances of OFETs, thin films of **DPP-2T2P-2DCV** displayed ambipolar semiconducting behavior in air, and μ_e and μ_h values reached 0.168 and 0.015 cm^2 V^{-1} s^{-1}, respectively. Inserting of phenylene groups to both sides of **DPP-T-DCV** molecule results in the increase of HOMO energy, which switches the transport characteristics from unipolar n-type conduction to ambipolarity. To our knowledge, this is the best result for solution processable ambipolar oligomeric semiconductors measured under ambient conditions. Further work will focus on molecule functionalization to modulate the intermolecular interactions for film morphology improvement as well as on the optimization of the devices by changing the substrate or electrode to achieve high-performance ambipolar OFET devices.

Acknowledgements

The authors acknowledge financial support from the National Natural Science Foundation of China (grant No.21062022) and the Natural Science Foundation of Jiangsu Province (BK2011408).

Notes and references

1 D. Voss, *Nature*, 2000, **407**, 442.
2 J. A. Rogers, Z. Bao, K. Baldwin, A. Dodabalapur, B. Crone, V. R. Raju, V. Kuck, H. Katz, K. Amundson, J. Ewing and P. Drzaic, *Proc. Natl. Acad. Sci. U. S. A.*, 2001, **98**, 4835.
3 G. Gelinck, P. Heremans, K. Nomoto and T. D. Anthopoulos, *Adv. Mater*., 2010, **22**, 3778.
4 Y. Guo, G. Yu and Y. Liu, *Adv. Mater*., 2010, **22**, 4427.
5 T. Someya, A. Dodabalapur, J. Huang, K. C. See and H. E. Katz, *Adv. Mater*., 2010, **22**, 3799.
6 P. Lin and F. Yan, *Adv. Mater*., 2012, **24**, 34.
7 H. Yan, Z. H. Chen, Y. Zheng, C. Newman, J. R. Quinn, F. Dotz, M. Kastler and A. Facchetti, *Nature*, 2009, **457**, 679.
8 H. Ebata, T. Izawa, E. Miyazaki, K. Takimiya, M. Ikeda, H. Kuwabara and T. Yui, *J. Am. Chem. Soc*., 2007, **129**, 15732.
9 M. J. Kang, I. Doi, H. Mori, E. Miyazaki, K. Takimiya, M. Ikeda and H. Kuwabara, *Adv. Mater*., 2011, **23**, 1222.
10 S. W. Yun, J. H. Kim, S. Shin, H. Yang, B.-K. An, L. Yang and S. Y. Park, *Adv. Mater*., 2012, **24**, 911.
11 Y. Zhao, C.-A. Di, X. Gao, Y. Hu, Y. Guo, L. Zhang, Y. Liu, J.Wang,W. Hu and D. Zhu, *Adv.Mater*., 2011, **23**, 2448.
12 Y. Mei, M. A. Loth, M. Payne, W. Zhang, J. Smith, C. S. Day, S. R. Parkin, M. Heeney, I. McCulloch, T. D. Anthopoulos, J. E. Anthony and O. D. Jurchescu, *Adv. Mater*., 2013, **25**, 4352.
13 I. Kang, H.-J. Yun, D. S. Chung, S.-K. Kwon and Y.-H. Kim, *J. Am. Chem. Soc.*, 2013, **135**, 14896.
14 T. Mori, T. Nishimura, T. Yamamoto, I. Doi, E. Miyazaki, I. Osaka and K. Takimiya, *J. Am. Chem. Soc*., 2013, **135**, 13900.
15 T. Lei, J.-H. Dou, X.-Y. Cao, J.-Y.Wang and J. Pei, *J. Am. Chem. Soc.*, 2013, **135**, 12168.
16 H. Sirringhaus, *Adv. Mater*., 2005, **17**, 2411.
17 S. R. Forrest, *Nature*, 2004, **428**, 911.
18 F. Garnier, R. Hajlaoui, A. Yassar and P. Srivastava, *Science*, 1994, **265**, 1684.
19 S. Allard, M. Forster, B. Souharce, H. Thiem and U. Scherf, *Angew. Chem., Int. Ed.*, 2008, **47**, 4070.
20 H. Minemawari, T. Yamada, H. Matsui, J. Tsutsumi, S. Haas, R. Chiba, R. Kumai, T. Hasegawa, *Nature*, 2011, **475**, 364.
21 K. Takimiya, S. Shinamura, I. Osaka, E. Miyazaki, *Adv. Mater*. 2011, **23**, 4347.
22 G. Giri, E. Verploegen, S. Mannsfeld, S. Atahan-Evrenk, D. Kim, S. Lee, H. Becerril, A. Aspuru-Guzik, M. Toney, Z, Bao, *Nature*, 2011, **480**, 504.
23 B. Naab, S. Himmelberger, Y. Diao, K. Vandewal, P. Wei, B. Lussem, A. Salleo, Z. Bao, *Adv. Mater*. 2013, **33**, 4663.
24 X. Chen, Y. Guo, L. Tan, G. Yang, Y. Li, G. Zhang, Z. Liu, W. Xu, D. Zhang, *J. Mater. Chem. C*, 2013, **1**, 1087.
25 J. Soeda, T. Uemura, Y. Mizuno, A. Nakao, Y. Nakazawa, A. Facchetti, J. Takeya, *Adv. Mater*. 2011, **23**, 3681.
26 F. Zhang, Y. Hu, T. Schuettfort, C. Di, X. Gao, C. McNeill, L. Thomsen, S. Mannsfeld, W. Yuan, H. Sirringhaus, D. Zhu, *J. Am. Chem. Soc*., 2013, **135**, 2338.
27 C. Kanimozhi, N. Yaacobi-Gross, K. Chou, A. Amassian, T. Anthopoulos, S. Patil, *J. Am. Chem. Soc.,* 2012, 134, 16532.
28 K.-J. Baeg, D. Khim, S.-W. Jung, M. Kang, I.-K. You, D.-Y. Kim, A. Facchetti and Y.-Y. Noh, *Adv. Mater*., 2012, **24**, 5433.

29 J. Zaumseil and H. Sirringhaus, *Chem. Rev*., 2007, **107**, 1296.
30 M. Muccini, *Nat. Mater*., 2006, **5**, 605.
31 F. Dinelli, R. Capelli, M. A. Loi, M. Murgia, M. Muccini, A. Facchetti and T. J. Marks, *Adv. Mater*., 2006, **18**, 1416.
32 R. Capelli, S. Toffanin, G. Generali, H. Usta, A. Facchetti and M. Muccini, *Nat. Mater*., 2010, **9**, 496–503.
33 Y. N. Li, S. P. Singh and P. Sonar, *Adv. Mater*., 2010, **22**, 4862.
34 T. L. Nelson, T. M. Young, J. Liu, S. P. Mishra, J. A. Belot, C. L. Balliet, A. E. Javier, T. Kowalewski and R. D. McCullough, *Adv. Mater*., 2010, **22**, 4617.
35 S. Cho, J. Lee, M. Tong, J. H. Seo and C. Yang, *Adv. Funct. Mater*., 2011, **21**, 1910.
36 H. Chen, Y. Guo, G. Yu, Y. Zhao, J. Zhang, D. Gao, H. Liu and Y. Liu, *Adv. Mater*., 2012, **24**, 4618.
37 J. D. Yuen, J. Fan, J. Sei□er, B. Lim, R. Hufschmid, A. J. Heeger and F. Wudl, *J. Am. Chem. Soc*., 2011, **133**, 20799.
38 H. Bronstein, Z. Chen, R. S. Ashraf, W. Zhang, J. Du, J. R. Durrant, P. Shakya Tuladhar, K. Song, S. E. Watkins, Y. Geerts, M. M. Wienk, R. A. J. Janssen, T. Anthopoulos, H. Sirringhaus, M. Heeney and I. McCulloch, *J. Am. Chem. Soc*., 2011, **133**, 3272.
39 S. Loser, C. J. Bruns, H. Miyauchi, R. P. Ortiz, A. Facchetti, S. I. Stupp and T. J. Marks, *J. Am. Chem. Soc*., 2011, **133**, 8142.
40 L. Dou, J. Gao, E. Richard, J. You, C.-C. Chen, K. C. Cha, Y. He, G. Li and Y. Yang, *J. Am. Chem. Soc*., 2012, **134**, 10071.
41 S. Qu and H. Tian, *Chem. Commun*., 2012, **48**, 3039.
42 L. Dou, J. You, J. Yang, C.-C. Chen, Y. He, S. Murase, T. Moriarty, K. Emery, G. Li and Y. Yang, *Nat. Photonics*, 2012, **6**, 180.
43 Y. N. Li, P. Sonar, L. Murphy and W. Hong, *Energy Environ. Sci*., 2013, **6**, 1684.
44 A. R. Mohebbi, J. Yuen, J. Fan, C. Munoz, M. f. Wang, R. S. Shirazi, J. Seifter and F. Wudl, *Adv. Mater*., 2011, **23**, 4644.
45 Z. Chen, M. J. Lee, R. Shahid Ashraf, Y. Gu, S. Albert-Seifried, M. Meedom Nielsen, B. Schroeder, T. D. Anthopoulos, M. Heeney, I. McCulloch and H. Sirringhaus, *Adv. Mater*., 2012, **24**, 647.
46 A. J. Kronemeijer, E. Gili, M. Shahid, J. Rivnay, A. Salleo, M. Heeney and H. Sirringhaus, *Adv. Mater*., 2012, **24**, 1558.
47 P. Sonar, S. P. Singh, Y. Li, M. S. Soh and A. Dodabalapur, *Adv. Mater*., 2010, **22**, 5409.
48 R. S. Ashraf, Z. Chen, D. S. Leem, H. Bronstein, W. Zhang. B. Schroeder, Y. Geerts, J. Smith, S. Watkins, T. D. Anthopoulos, H. Sirringhaus, J. C. de Mello, M. Heeney and I. McCulloch, *Chem. Mater*., 2010, **23**, 768.
49 J. Lee, A.-R. Han, J. Kim, Y. Kim, J. H. Oh and C. Yang, *J. Am. Chem. Soc*., 2012, **134**, 20713.
50 Y. Zhang, C. Kim, J. Lin and T.-Q. Nguyen, *Adv. Funct. Mater*., 2012, **22**, 97.
51 Y. Suna, J.-I. Nishida, Y. Fujisaki and Y. Yamashita, *Org. Let*t., 2012, **14**, 3356.
52 Y. Wang, Q. Huang, Z. Liu and H. Li, *RSC Adv.*,2014, **4**,29509–29513.
53 A. Riaño, P. Mayorga Burrezo, M. J. Mancheño, A. Timalsina, J. Smith, A. Facchetti, T. J. Marks, J. T. Lõpez Navarrete, J. L. Segura, J. Casadob and R. Ponce Ortiz, *J. Mater. Chem. C*, 2014, **2**, 6376.
54 Z. Cai, H. Luo, X. Chen, G. Zhang, Z. Liu, and D. Zhang, *Chem. Asian J*., 2014, **9**, 1068.
55 L. Wang, X. Zhang, H. Tian, Y. Lu, Y. Geng and F. Wang, *Chem. Commun*., 2013, **49**, 11272.
56 W. S. Yoon, S. K. Park, I. Cho, J.-A. Oh, J. H. Kim, and S. Y. Park, *Adv. Funct. Mater*. 2013, **23**, 3519.
57 B. P. Karsten, J. C. Bijleveld and R A. J. Janssen, *Macromol. Rapid Commun*., 2010, **31**, 1554–1559
58 M. Mas-Torrent and C. Rovira, *Chem. Soc. Rev*., 2008, **37**, 827